Imaging Terrestrial Planets with a Free Flying Occulter and Space Telescope: An Optical Simulation

A. B. Schultz[a], R. G. Lyon[b], M. Kochte[a], D. Fraquelli[a], F. Bruhweiler[c], I. J. E. Jordan[a], K. G. Carpenter[b], M. DiSanti[b], C. Miskey[c], M. Rodrigue[d], M. S. Fadali[e], D. Skelton[f], H. M. Hart[g], and K.-P. Cheng[h]

[a]Science Programs, Computer Sciences Corporation, and the Space Telescope Science Institute, 3700 San Martin Drive, Baltimore, MD 21218

[b]NASA's Goddard Space Flight Center, Greenbelt, MD 20771

[c]Department of Physics, Catholic University of America, Washington, DC 20064

[d]Department of Physics, University of Nevada, Reno, NV 89557-0058

[e]Department of Electrical Engineering, University of Nevada, Reno, NV 89557-6627

[f]Orbital Sciences Corporation, 7500 Greenway Center Drive, Suite 700, Greenbelt, MD 20770

[g]Science Programs, Computer Sciences Corporation, and The Johns Hopkins University, Baltimore, MD 21218

[h]Department of Physics, California State University Fullerton, Fullerton, CA 92634

ABSTRACT

In this manuscript, we further develop our concepts for the free-flying occulter space-based mission, Umbral Missions Blocking Radiating Astronomical Sources (UMBRAS). Our optical simulations clearly show that an UMBRAS-like mission designed around a 4-m telescope and 10-m occulter could directly image terrestrial planets. Such a mission utilizing existing technology could be built and flown by the end of the decade. Moreover, many of the other proposed concepts for Terrestrial Planet Finder (TPF) could significantly benefit by using an external occulter.

We present simulations for an optical design comprising a square aperture telescope plus square external occulter. We show that the entire diffraction pattern, which is propagated from occulter to telescope and through telescope to focal plane, may be characterized by two parameters, the Fresnel number and the ratio of the telescope diameter to the occulter width. Combining the effects of a square occulter with apodization provides a much more rapid roll-off in the PSF intensity between the diffraction spikes than may be achieved with an unapodized telescope aperture and occulter. We parameterize our results with respect to wavefront quality and compare them against other competing methods for exo-planet imaging. The combination of external occulter and apodization yields the required contrast in the region of the PSF essential for exo-planet detection. An occulter external to the telescope (i.e., in a separate spacecraft, as opposed to a classical coronagraph with internal occulter) reduces light scatter within the telescope by approximately 2 orders of magnitude. This is due to less light actually entering the telescope. Reduced scattered light significantly relaxes the constraints on the mirror surface roughness, especially in the mid-spatial frequencies critical for planet detection. This study, plus our previous investigations of engineering as well as spacecraft rendezvous and formation flying, clearly indicates that the UMBRAS concept is very competitive with, or superior to, other proposed concepts for TPF missions.

Keywords: Exo-planet detection, coronagraph, occulter, space telescope

Al Schultz is an Instrument Scientist at the Space Telescope Science Institute (STScI). He has worked at STScI for ∼13 years. Since launch, Dr. Schultz has supported HST operations in PODPS, which is now part of OPUS, the GHRS, STIS, NICMOS, and WFPC2 instruments. (Send correspondence to schultz@stsci.edu; Telephone: 410-338-5044)

1. INTRODUCTION

One of the "Holy Grails" of astrophysics is the detection of earth-like planets around nearby stars. So far, radial velocity studies of nearby solar-type stars have discovered over 100 Jupiter-sized planets (see papers by Mayor, Queloz, Marcy, Butler, Fisher, Noyes, Cochran, Hatzes, and many more investigators, too many to be listed here). Thus, there are more than 10 times the number of known planets outside as inside our solar system. Some systems are unlike our own Solar System in that they are dominated by giant, Jupiter-like planets, orbiting within a fraction of an A.U. of the primary.

Direct imaging has the potential to detect both Jupiter and Earth-like planets at large distances from their primaries. Visually, planets shine by reflected starlight, making them difficult to image against the glare of their parent stars. Current direct imaging capabilities are limited to ground-based coronagraphic and adaptive optics (AO) imaging with 8-m or larger telescopes[1] and with the instruments onboard the Hubble Space Telescope (HST).[2] To date, none of these platforms has imaged any verifiable exo-planet.

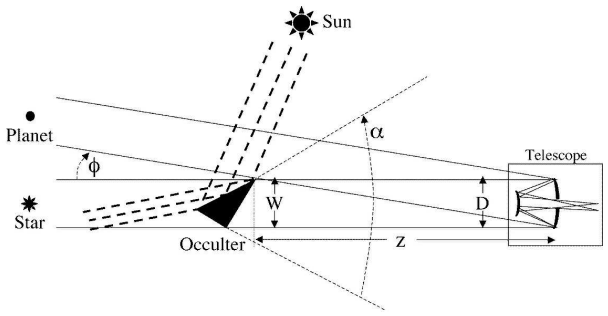

Figure 1. Relative configuration of an occulter operating with a space telescope. The view is from above the plane containing the Sun, occulter, and telescope. The separation and sizes of the occulter and telescope are not to scale.

Our previous studies have shown free-flying occulters in combination with a space-based telescope are a promising means to image and study nearby exo-planets.[3–5] Figure 1 presents the formation configuration of a coronagraphic system consisting of an external free-flying occulter and space telescope. At optical wavelengths, conventional Lyot coronagraphs have, at best, achieved contrast enhancements of $\sim 10^4$ in the 5-10 Airy ring annulus[6] . Simulations of an apodized square aperture space telescope suggest that a contrast enhancement of $\sim 10^6$ could be achieved in the same annular region. Further simulations of an apodized square aperture telescope in combination with a free-flying square occulter indicate that the contrast enhancement could be boosted to $\geq 10^8$. Since a terrestrial planet, in reflected light, is typically 10 orders of magnitude dimmer than the central star, i.e. the luminosity ratio of the planet to star is 10^{-10}, a space-based apodized telescope plus external occulter system should be able to directly image terrestrial planets.

2. OPTICAL MODELING

Optical simulation of an external occulter and a space telescope is a two step process modeling Fresnel diffraction from the occulter to the telescope aperture and Fraunhofer diffraction from the aperture to the focal plane. Fresnel diffraction occurs because the diffracting obstruction (occulter) is at a finite distance from the telescope entrance pupil plane. Figure 2 shows a schematic of the system. Herein we derive the equations for propagation of the electric field from the occulter to the telescope entrance pupil and subsequently through to the telescope focal plane.[7,8]

2.1. Occulter to Focal Plane Propagation

Free space propagation of the scalar electric field is described by the spatial Helmholtz wave equation with appropriate boundary conditions:

$$\bigtriangledown^2 E(\vec{r}) + k^2 \varepsilon E(\vec{r}) = 0 \tag{1}$$

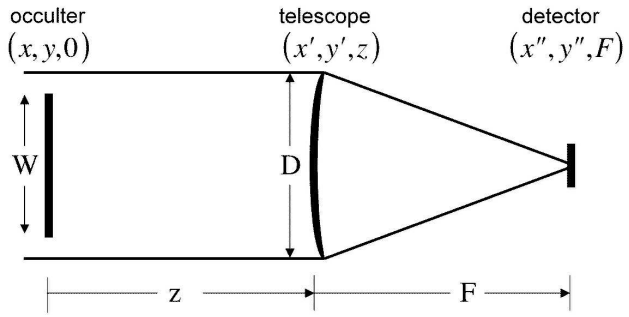

Figure 2. Simplified Schematic of External Occulting Coronagraph. Light from a stellar source is diffracted by the occulter and is intercepted by the telescope entrance pupil. The telescope both changes the phase and amplitude, then focuses the source at the detector plane.

where $\vec{r} = (x, y, z)$ is a point in space, $E(\vec{r})$ is the scalar electric field at that point, and $k = 2\pi/\lambda$ and $\varepsilon = 1$ are the wavenumber and permitivity in free space, respectively, where λ is the wavelength.

Equation (1) can be reduced from a 2^{nd} order partial differential equation to a 2^{nd} order ordinary differential equation for planar boundary conditions. If we let the planar boundary conditions be oriented along the $x - y$ plane, then equation (1) can be written as:

$$\left[-4\pi^2(f_x^2 + f_y^2) + \frac{4\pi^2}{\lambda^2}\right] E(f_x, f_y, z) + \frac{\partial^2}{\partial z^2} E(f_x, f_y, z) = 0 \tag{2}$$

where (f_x, f_y) are the Fourier conjugate variables (spatial frequencies) to (x, y). The solution to (2) is given by:

$$E(f_x, f_y, z) = E(f_x, f_y, 0) e^{-i\frac{2\pi}{\lambda} z \sqrt{1-\lambda^2(f_x^2+f_y^2)}} \tag{3}$$

i.e., the *angular spectrum* representation. For planar boundary conditions free space propagation is as simple as taking the Fourier transform of the boundary conditions, multiplying by a phasor, and applying the inverse Fourier transform. In practice numerical evaluations of (3) for larger "z" are difficult due to the required large computational array sizes. For solutions to the field close to the z-axis, we can adopt the Fresnel approximation by applying a binomial expansion to the square root term in equation (3) and keeping only the first two terms:

$$\sqrt{1 - \lambda^2(f_x^2 + f_y^2)} \approx 1 - \frac{\lambda^2}{2}(f_x^2 + f_y^2) \tag{4}$$

We reverse the order of integration using the integral of equation (3) to yield the Fresnel integral:

$$E(x', y', z) = \frac{-i}{\lambda z} e^{-i\frac{2\pi}{\lambda} z} \iint dx dy \, E(x, y, z) \, e^{-i\frac{\pi}{\lambda z}\left[(x-x')^2 + (y-y')^2\right]} \tag{5}$$

The electric field at the occulter plane can be modeled as:

$$E(x, y, 0) = E_0 \left\{1 - \Phi(x, y, W)\right\} \tag{6}$$

where E_0, the electric field amplitude incident on the occulter, is assumed to be constant for a point source at infinity. Here, $\Phi(x, y, W)$ is the shape function of the occulter and is unity within the occulter and zero elsewhere. This type of occulter is essentially a planar blocking mask of width "W".

Propagation to the telescope entrance pupil is given by inserting (6) into the Fresnel integral (5) and evaluating:

$$E(x', y', z) = E_0 e^{-ikz} \left\{-1 + \frac{i}{\lambda z} \iint dx dy \Phi(x, y, W) \, e^{-i\frac{\pi}{\lambda z}\left[(x-x')^2 + (y-y')^2\right]}\right\} \tag{7}$$

The electric field at the telescope entrance pupil is seen to be the difference of two terms: (i) a plane wave that would exist without the occulter and (ii) a defocussed (quadratic phase factor in integral) Fourier transform of the occulter shape function.

The apodized pupil function of the telescope can be modeled as the electric field transmittance $T(x', y')$ where $T(x', y')$ is zero outside the telescope pupil and is less than or equal to unity, depending on choice of apodization function.

Propagating the electric field from the entrance pupil to the focal plane is accomplished by the Fraunhofer integral for the focusing system:

$$E(x'', y'', F) = \frac{-i}{\lambda F} e^{-i\frac{\pi}{\lambda F}\left[x''^2 + y''^2\right]} \iint dx'dy'\, T(x', y') E(x', y', z) e^{-i\frac{2\pi}{\lambda F}(x'x'' + y'y'')} \tag{8}$$

Inserting equation (7) into equation (8) gives a single expression for the focal plane point spread function (PSF):

$$PSF(x'', y'') = \left| ASF(x'', y'') - ASF(x'', y'') * *FT^{-1}\left\{FP\left[\Phi(x, y, W)\right]\right\}\right|^2 \tag{9}$$

where ASF is the amplitude spread function; i.e., the Fourier transform of the 2D apodized pupil function. FP represents Fresnel propagation and FT represents Fourier transform. The inverse Fourier transform of the Fresnel propagated occulter shape function will give a blurred image of the occulter in the focal plane. This convolved with the ASF will spread the blur even larger. Subtracting this from the ASF will remove the core and some of the wing structure of the PSF. Combining this with pupil apodization will cause an even greater increase in contrast.

2.2. Circular Symmetry

If we assume a circular occulter with radius of R and a circular telescope with diameter D, then equation (7) can be simplified to a 1D integral. With circular symmetry the 2^{nd} term in equation (7) defined by:

$$I_2 = \iint dxdy\, \Phi(x, y)\, e^{-i\frac{\pi}{\lambda z}(x^2 + y^2)} e^{-i\frac{2\pi}{\lambda z}(xx' + yy')} \tag{10}$$

with the definitions:

$$x \equiv rcos(\theta) \text{ and } y \equiv rsin(\theta)$$
$$x' \equiv \rho cos(\phi) \text{ and } y' \equiv \rho sin(\phi)$$

becomes:

$$I_2 = \iint rd\theta dr\, \Phi(r)\, e^{-i\frac{\pi}{\lambda z}r^2} e^{-i\frac{2\pi}{\lambda z}r\rho(cos\theta cos\phi + sin\theta sin\phi)} \tag{11}$$

and using:

$$cos\theta cos\phi + sin\theta sin\phi = sin(\theta - \phi)$$

yields:

$$I_2 = \iint rd\theta dr\, \Phi(r)\, e^{-i\frac{\pi}{\lambda z}r^2} e^{-i\frac{2\pi}{\lambda z}r\rho sin(\theta - \phi)} \tag{12}$$

Rearranging the terms gives:

$$I_2(R) = \int_0^R rdr\, e^{-i\frac{\pi}{\lambda z}r^2} \int_0^{2\pi} d\theta\, e^{i\frac{2\pi}{\lambda z}r\rho sin(\theta - \phi)} \tag{13}$$

Evaluating the 2^{nd} integral (Abramowitz and Stegun) yields:

$$I_2(\rho, R) = 2\pi \int_0^R rdr\, e^{-i\frac{\pi}{\lambda z}r^2} J_0(\frac{2\pi\rho}{\lambda z}) \tag{14}$$

Assuming circular symmetry, equation (7) becomes:

$$E(\rho, z, R) = E_0\, e^{-ikz} \left\{ -1 + \frac{i2\pi}{\lambda z} e^{-i\frac{\pi}{\lambda z}\rho^2} \int_0^R r dr\, e^{-i\frac{\pi}{\lambda z}r^2} J_0(\frac{2\pi\rho}{\lambda z}) \right\} \tag{15}$$

where ρ is the radial coordinate in plane of the exit pupil of the telescope and R is the radius of the occulter. Equation (15) can be evaluated with 1D quadrature for each value of ρ.

2.3. Square Symmetry

For a square occulter and a square aperture telescope, equation (7) is separable into 2 integrals, 1 per dimension, of the form:

$$E(x', y', z) = E_0 e^{-ikz} \left\{ -1 + \frac{i}{\lambda z} \int_{-W/2}^{W/2} dx\, e^{-i\frac{\pi}{\lambda z}(x-x')^2} \int_{-W/2}^{W/2} dy\, e^{-i\frac{\pi}{\lambda z}(y-y')^2} \right\} \tag{16}$$

and using the definitions of Fresnel integrals (Abramowitz and Stegun):

$$C(x) = \int_0^x dt\, cos(\frac{\pi}{2}t^2)\ and\ S(x) = \int_0^x dt\, sin(\frac{\pi}{2}t^2) \tag{17}$$

to yield (details to be presented elsewhere):

$$E(x', y', z) = E_0 e^{-ikz} \left\{ -1 + \frac{i}{2} \left[U(y') - iV(y')\right] \left[U(x') - iV(x')\right] \right\} \tag{18}$$

where:

$$U(x') \equiv C\left(\sqrt{\frac{2}{\lambda z}}\left(\frac{W}{2} + x'\right)\right) + C\left(\sqrt{\frac{2}{\lambda z}}\left(\frac{W}{2} - x'\right)\right) \tag{19}$$

$$V(x') \equiv S\left(\sqrt{\frac{2}{\lambda z}}\left(\frac{W}{2} + x'\right)\right) + S\left(\sqrt{\frac{2}{\lambda z}}\left(\frac{W}{2} - x'\right)\right) \tag{20}$$

Thus, the electric field at the telescope's entrance pupil is seen to be a combination of Fresnel integrals which can be evaluated by standard numerical methods (see e.g. Abramowitz and Stegun, pg 299, equation 7.1.29, or Numerical Recipes in C). Equation (18) is symmetric in both x and y since $U(-x') = U(x')$ and $V(-x') = V(x')$. The shape of the field at the telescope is dependent only on the Fresnel number defined by $F_N \equiv W^2/\lambda z$. The Fresnel number is a dimensionless parameter where W is the characteristic width of the mask ("occulter"), λ is the wavelength, and z is the distance of the occulter from the aperture. The $F_N \ll 1$ regime is called Fraunhofer diffraction, while $F_N \geq 1$ produces Fresnel diffraction. Intermediate regimes require more difficult analysis, but can be treated using scalar diffraction theory.

If we look at the form of (18) at the origin, i.e. $x' = y' = 0$, then $U(0) = 2C\left(\sqrt{\frac{W^2}{2\lambda z}}\right)$ and $V(0) = 2S\left(\sqrt{\frac{W^2}{2\lambda z}}\right)$ to give:

$$E(0, 0, z) = E_0 e^{-ikz} \left\{ -1 + 2i \left\{ C\left(\sqrt{\frac{W^2}{2\lambda z}}\right) - iS\left(\sqrt{\frac{W^2}{2\lambda z}}\right) \right\}^2 \right\}. \tag{21}$$

Thus, the relative intensity is given by:

$$\frac{I}{I_0} = \left| -1 + 2i \left\{ C\left(\sqrt{\frac{W^2}{2\lambda z}}\right) - iS\left(\sqrt{\frac{W^2}{2\lambda z}}\right) \right\}^2 \right|^2 \tag{22}$$

where I_0 is the intensity of the plane wave incident on the occulter.

3. OPTICAL SIMULATIONS

A series of computer simulations were conducted to evaluate Equation 9, the expression for the focal plane point spread function (PSF). The diffraction propagation results for the fields and intensity at the telescope entrance pupil are presented in the Section "On-Axis Intensity at Telescope Pupil" and in the focal plane of the telescope in the Section "Telescope Point Spread Function (PSF)." We show that the energy distribution is favorable, yielding an increase in the planet-to-stellar contrast.

3.1. On-Axis Intensity at Telescope Pupil

The on-axis relative intensity at the telescope pupil, Equation 22, is evaluated and presented in Figure 3 plotted versus Fresnel Number (F_N). The on-axis relative intensity falls rapidly for increasing F_N, as the occulter moves closer to the telescope. At the position of the occulter, the intensity would be zero. Notice that periodic nulls occur in the intensity. These nulls will be smeared out for increasing spectral bandwidth. This relation, along with the telescope size (i.e. required resolution and sensitivity), defines the size of the occulter, telescope, and its distance from the occulter.

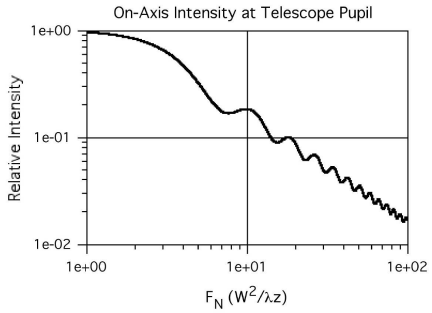

Figure 3. On-axis relative intensity versus F_N. The intensity is "measured" at the telescope aperture.

We next evaluate the mean relative intensity for a square occulter in the plane of the telescope pupil. Figure 4 shows how the amount of starlight entering the telescope varies with differing ratios of the telescope diameter to occulter width (D/W). The reduced amount of light entering the telescope and the corresponding reduction in light scatter indicates that the required optical surface smoothness is only $\lambda/100$ to $\lambda/200$, well within the capability of current technology, and much more relaxed than that required for other SIM[9] and TPF[10] mission concepts.

Once the telescope size exceeds the occulter size ($D/W > 1$), there is little gain in an external occulter over an internal occulter since most of the starlight reaches the telescope. Also in Figure 4 is a plot showing the intensity distribution of the starlight entering the telescope. The intensity distribution becomes increasingly complex for increasing Fresnel number, as the occulter moves closer to the telescope. Correspondingly, Figure 5 presents the calculated images of the wavefront. At larger Fresnel numbers, the telescope falls increasingly into the shadow of the occulter. Note that using the Fresnel number (F_N) and $\sqrt{\lambda z}$ as units allows us to use parameters without adopting a specific system size or distance of propagation.

The intensity may be further reduced by apodizing the telescope. Figure 6 shows the relative intensity averaged across the entrance pupil of the telescope, when apodization is applied at the telescope entrance pupil. As expected, apodization lowers the mean intensity ~ 1 order of magnitude. Although the light from a planet is also reduced by the same amount, there is a net gain since the diffracted light outside the stellar PSF core is reduced. Combining an occulter with apodization allows us to redistribute the energy, reshaping the final image and concentrating more energy into the core of the stellar PSF.

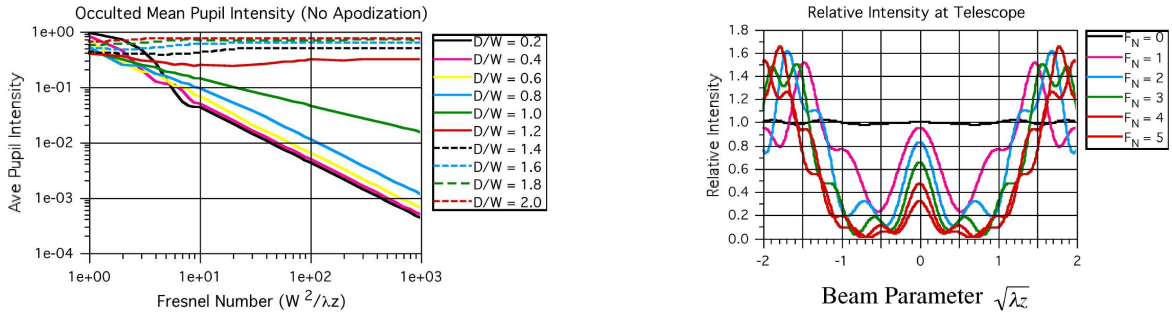

Figure 4. Left, Mean Relative Intensity at Telescope Entrance Pupil vs. Fresnel Number. Right, Relative Intensity at Telescope Entrance Pupil vs Beam Parameter. Intensity is nearly uniform in the far-field ($F_N \sim 1$) and shows increasingly complex behavior as the occulter and telescope are moved increasingly into the Fresnel domain (closer spacing).

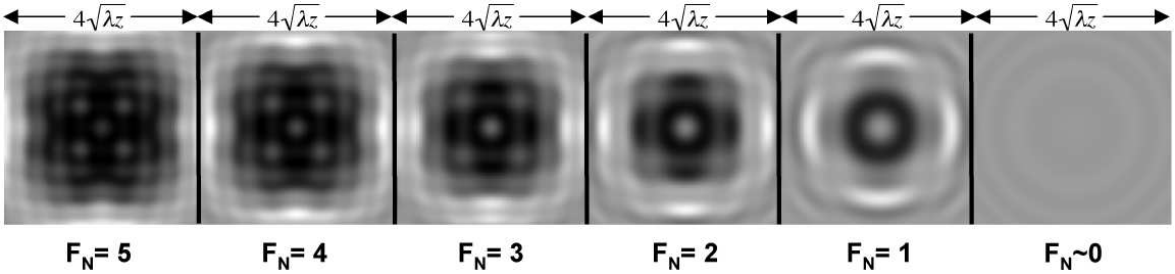

Figure 5. Illustrative Plots of Relative Intensity at Telescope Entrance Pupil. For larger F_N, the shadow of the square occulter emerges but becomes more uniform with decreasing F_N, as the occulter moves to the far field.

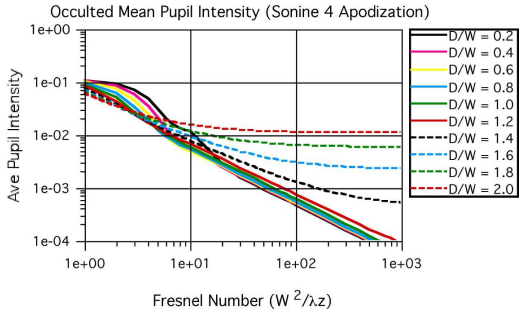

Figure 6. Mean Relative Intensity at Apodized Telescope Entrance Pupil vs Fresnel Number.

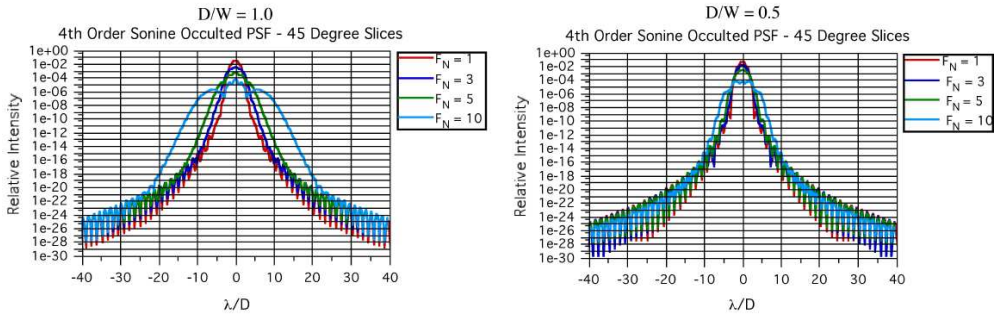

Figure 7. Apodized Point Spread Functions (PSFs). Left, PSFs for $D/W = 1$. Right, PSFs for $D/W = 0.5$. Ten orders of magnitude reduction in PSF can be achieved as close as $\sim 3\lambda/D$.

3.2. Telescope Point Spread Function (PSF)

We now evaluate Equation 9 at the focal plane of the telescope for the special case of a square occulter and a square aperture telescope with and without apodization applied. Figure 7 shows two sets of plots. The left set is for an occulter and telescope of the same size and the right set for a telescope 1/2 the size of the occulter. From these plots, it is evident that the intensity of the PSF can be reduced to below 10^{-10} as close as $\sim 3\lambda/D$ for some parameter combinations. This is quite interesting since it shows that the free-flying occulter and apodized telescope are a viable candidate architecture for imaging terrestrial planets around the nearby stars.

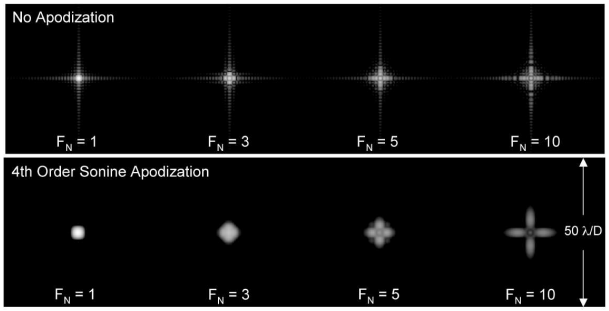

Figure 8. Un-Apodized and Apodized Point Spread Function (PSF) with $D/W = 1.0$.

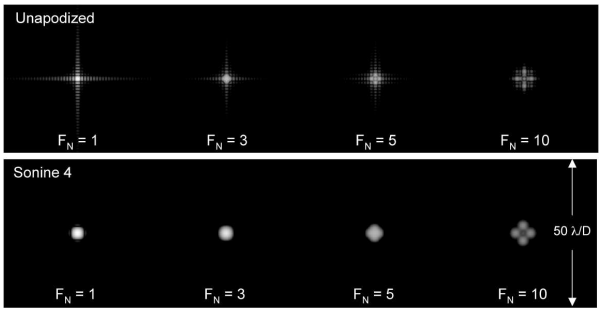

Figure 9. Un-Apodized and Apodized Point Spread Functions (PSF) with $D/W = 0.5$.

Figures 8 and 9 show the PSFs for $D/W = 1.0$ and $D/W = 0.5$ respectively. Figure 8, top and bottom rows show the PSFs without and with apodization respectively, for a square occulter and square telescope, for

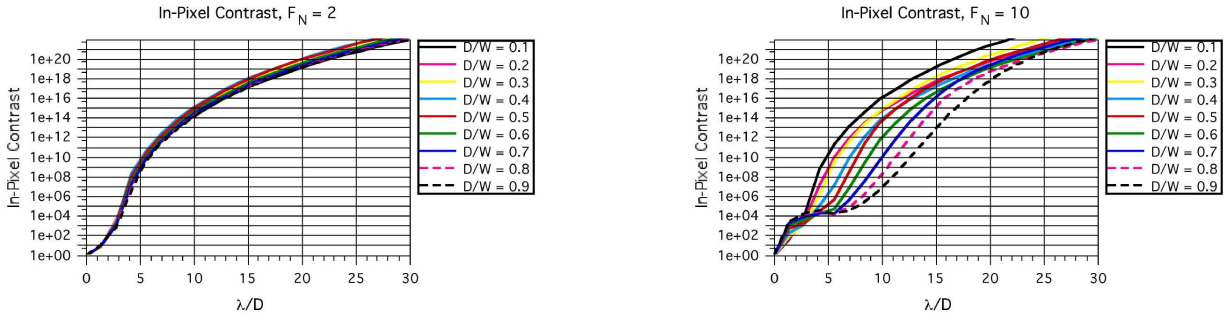

Figure 10. The ratio of the stellar flux to the planetary flux in a $(\lambda/D)^2$ pixel as a function of angular separation between the planet and star. As D/W increases, the contrast decreases for a given separation. Note that for $D/W = 0.1$ and $F_N = 10$, high contrast is achieved at smaller separations (λ/D).

a telescope of $D/W = 1$. Figure 9, top and bottom rows show the PSFs without and with apodization for a telescope of $D/W = 0.5$. Both Figures 8 and 9 vary in Fresnel number from 1 to 10 from left to right.

Figure 10 shows the *in-pixel contrast*, i.e. the ratio of the star flux to the planetary flux in a $(\lambda/D)^2$ pixel, as a function of angular separation between the planet and star. Two sets of plots are shown for F_N equal 2 (left) and 10 (right), respectively. On each plot, the ratio of telescope size to occulter width (D/W) ranges from 0.1 to 0.9. Inspection shows that for $F_N = 2$, the contrast exceeds 10^{10} for angular separations $\geq 5\lambda/D$ and is nearly independent of D/W. At $F_N = 10$, the contrast exceeds 10^{10} for angular separations greater than $\sim 4\lambda/D$ and the contrast is a stronger function of D/W. We find, at even higher Fresnel numbers, the contrast exceeds 10^{10} as close as $\sim 3\lambda/D$. These results show that systems with HST-like optics (surface roughness $\lambda/100$ to $\lambda/200$) and corresponding light scatter should detect earth-like planets as close as $\sim 4\lambda/D$.[6] For a 4-m telescope at 5500 Å , $\lambda/D = 0.028''$.

The actual detection contrast for terrestrial planets is obtained by multiplying the luminosity ratio by the "in-pixel contrast" (Figure 10). Thus at 6 Airy rings $(6\lambda/D)$, we would expect a contrast of ~ 100; the terrestrial planet would appear to be ~ 100 times brighter than the stellar background due to diffracted and scattered light. At 5 Airy rings, we would expect a contrast of $\sim 1 - 10$.

4. SUMMARY AND CONCLUSIONS

We have developed analytical and computational models for an apodized free-flying occulter and space-based telescope. The results presented herein are for perfect optics, i.e. no deformations, misalignments, light scatter, micro-roughness, transmission errors, or polarization effects are included. For the idealized case, this method of imaging planets is comparable to other proposed methods, which include an apodized aperture telescope, internal coronagraph, and space interferometry.

Studying terrestrial and giant planets about stars is one of the primary goals of NASA's Origins Program. There have been many different methods proposed to directly detect (image) and obtain low-resolution spectroscopy of exo-planets, terrestrial as well as Jovian type planets. These include space interferometry, space-based filled-aperture telescopes (apodized aperture or internal coronagraph), and ground-based adaptive optics (AO). A space-based free-flying occulter type mission has several important advances when compared to the existing proposed missions; (i) starlight is reduced before entering the telescope, (ii) light scatter within the telescope is reduced due to less star light entering the telescope as well as fewer obstructions within the telescope, and (iii) the optical tolerances are reduced to existing current technology HST-type optics. We suggest that a free-flying occulter and space-based telescope combination, for the purpose of detecting and studying exo-planets, can be built and launched with existing technology by the end of the decade with a minimum amount of development.

ACKNOWLEDGMENTS

The analytical and computational modeling were performed at NASA, Goddard Space Flight Center (GSFC), Greenbelt, MD using the Optical Systems Characterization and Analysis Research (OSCAR) software package.

We would like to thank Dr. Jan M. Hollis (NASA/GSFC) for his encouragement and support in completing this investigation. Support for this work has been provided by Computer Sciences Corporation, Laurel, MD and by the Space Telescope Science Institute which is operated by the Association of Universities for Research in Astronomy, Inc., under NASA contract NAS 5-26555.

REFERENCES

1. N. Siegler, L. M. Close, and M. Freed, *Guiding on the Edge ($V \sim 19$): Results from an AO Survey of Very Low Mass Stars Searching for Extremely Faint Companions*, in Adaptive Optical System Technologies II, P. L. Wizinowich, D. Bonaccini, Proc. of SPIE Vol. 4839, 114, 2002.
2. G. Schneider and M. D. Silverstone, *Coronagraphy with HST: detectability is a sensitive issue*, in High-Contrast Imaging for Exo-Planet Detection, A. B. Schultz, R. G. Lyon, eds., Proc. of SPIE Vol. 4860, 1, 2002.
3. A. B. Schultz, D. J. Schroeder, I. Jordan, F. Bruhweiler, M. A. DiSanti, H. M. Hart, F. C. Hamilton, J. Hershey, M. Kochte, C. L. Miskey, K. P. Cheng, M. Rodrigue, B. Johnson, and S. Fadali, *Imaging Planets About Other Stars with UMBRAS*, in Infrared Spaceborne Sensing VII, M. Strojnik, B. Andresen, eds., Proc. of SPIE Vol. 3759, 49, 1999.
4. A. B. Schultz, I. Jordan, H. M. Hart, F. Bruhweiler, D. A. Fraquelli, F. C. Hamilton, J. Hershey, M. Kochte, M. A. DiSanti, C. L. Miskey, K.-P. Chen, M. Rodrigue, B. Johnson, and M. S. Fadali, *Imaging Planets About Other Stars with UMBRAS II*, in Infrared Spaceborne Remote Sensing VIII, M. Strojnik, B. Andresen, eds. Proc. of SPIE Vol. 4131, 132, 2000.
5. A. B. Schultz, I. Jordan, M. Kochte, D. Fraquelli, F. Bruhweiler, J. M. Hollis, K. G. Capenter, R. G. Lyon, M. A. DiSanti, C. L. Miskey, J. Leitner, R. D. Burns, S. R. Starin, M. Rodrigue, S. Fadali, D. Skelton, H. M. Hart, F. C. Hamilton, and K. P. Cheng, *UMBRAS: A Matched Occulter and Telescope for Imaging Extrasolar Planets*, in High-Contrast Imaging for Exo-Planet Detection, A. B. Schultz, R. G. Lyon, eds., Proc. of SPIE Vol. 4860, 54, 2002.
6. R. G. Lyon, J. M. Hollis, and J. E. Dorband, *Comparative Optical Analysis of Extra-Solar Planetary Imaging Techniques*, in High-Contrast Imaging for Exo-Planet Detection, A. B. Schultz, R. G. Lyon, eds., Proc. of SPIE Vol. 4860, 251, 2002.
7. A. B. Schultz, *Studies of the Resolving Power of UNR's 16-inch Reflecting Telescope*, PhD Dissertation, University of Nevada, Reno, NV, 1982.
8. A. B. Schultz, T. V. Frazier, and E. Kosso, *Sonine's Bessel identity applied to apodization*, Applied Optics, 23, 1914, 1984.
9. R. Danner, S. Unwin, and R. J. Allen, *SIM: Space Interferometry Mission: Taking the Measure of the Universe*, Washington, DC:, NASA, 1999.
10. C. A. Beichman, *Terrestrial Planet Finder: the search for life-bearing planets around other stars*, Proc. SPIE Vol. 3350, 719, 1998.